Catalysis Today 156 (2010) 316–321

Contents lists available at ScienceDirect

Catalysis Today

journal homepage: www.elsevier.com/locate/cattod

Nanofiber membranes—Evaluation of gas transport

Karel Soukup*, David Petráš, Petr Klusoň, Olga Šolcová

Institute of Chemical Process Fundamentals of the ASCR, v.v.i., Rozvojová 135, CZ-165 02 Prague 6, Czech Republic

ARTICLE INFO

Article history:
Available online 17 June 2010

Keywords:
Nanofibers
Graham's diffusion cell
Gas diffusion
Electrospinning
Membranes

ABSTRACT

This work has been focused on the electrospinning generation of nanofibrous membranes from polystyrene and polyurethane, and on sandwich membranes composed of these two polymeric components, on their structural characterization and finally on the evaluation of their gas transport behaviour. These tests were based on the isothermal counter-current gas diffusion measurements in the Graham's diffusion cell. It was shown that the transport characteristics (the net diffusion molar flux densities) can be utilized for the control of the electrospinning process—homogeneity of the prepared membranes and their diffusion resistance.

1. Introduction

In the recent past considerable attention has been paid to the preparation, characterization and practical utilization of many various nanofibers [1–17]. Nanofibers have been produced in a number of principally different methods. However, the most common reported methodology is based on the electrospinning process [2,19–23]. Nonwoven mats prepared by this process revealing the submicron fibers typically exhibit large surface area per unit mass and also very high macroporosity. Density of these materials is usually very low (plastic material commonly 0.01–0.1 g/cm^3).

It is assumed that such structures can be used in a very broad range of applications, e.g. in catalysis, filtration, tissue engineering, wound care. Especially, in heterogeneous catalysis nanofiber systems (membranes) seem to be promising porous carriers for immobilization of the homogeneous catalysts based on the biopolymer compounds [1–3]. Immobilization on the nonwoven mats allows an accuracy controlling the catalytic activity and accessibility of the catalyst as well as its retrieval for the reaction mixture to a very high yield. Sufficiently high specific surface area (ranging from 1 to 35 m^2/g depending on the fibers diameter) together with generally low transport resistance of nanofibrous membranes competes with traditionally supported porous catalysts. Ebert et al. [4] tested palladium doped nanoparticles on electrospun nanofibers based on the poly(amideimide) in the hydrogenation of methyl oleate. They found about seven times higher catalytic activity for the nanofibrous catalytic system in comparison with a commercial Pd/Al_2O_3 catalyst. Demir et al. [5] focused on the catalytic activity of palladium nanoparticles on electrospun nanofibers consisted of acrylic acid and acrylonitrile copolymer. For hydrogenation of dehydrolinalool 4.5 times higher catalytic activity for the nanofibrous system compared to Pd/Al_2O_3 catalyst was found. These results confirmed the nanofibrous membranes as promised supports owing to their fine porous structure, good pores interconnectivity, a high specific surface area and the appropriate transport properties (generally low diffusion resistance).

Studies on electrospinning have been mostly focused on morphological characteristics (based on the SEM image analysis) of the electrospun membranes (e.g. [6–13]), while only a few studies [14–18] have been published on determination of the transport properties. It must be noted that membranes prepared from the layered nanofibers reveal enhanced transport properties useful for catalytic processes as well as various separation systems. These parameters depend on the fiber diameter, thickness of a membrane, weight per a unit area, etc.

This paper reports on the preparation of polystyrene (PS) and polyurethane (PU) nanofiber membranes, their structural description and their counter-current gas diffusion characteristics. The transport properties are first provided for each of the membrane types separately then a sandwich PU–PS–PU structure is produced and described analogously. It is believed that this knowledge (not reported before), might be of special importance for any practical utilization of this kind of new unique materials.

2. Experimental

2.1. Nanofiber layer preparation

Polystyrene granulate (Krasten 137, Kaučuk-Unipetrol Group) was dissolved in a mixed solvent of methylisobutylketone p.a.

* Corresponding author at: Institute of Chemical Process Fundamentals of the ASCR, v.v.i., Rozvojová 135, CZ-165 02 Prague 6, Czech Republic. Tel.: +420 220 390 282; fax: +420 220 920 661.
E-mail address: soukup@icpf.cas.cz (K. Soukup).

0920-5861/$ – see front matter © 2010 Elsevier B.V. All rights reserved.
doi:10.1016/j.cattod.2010.05.016

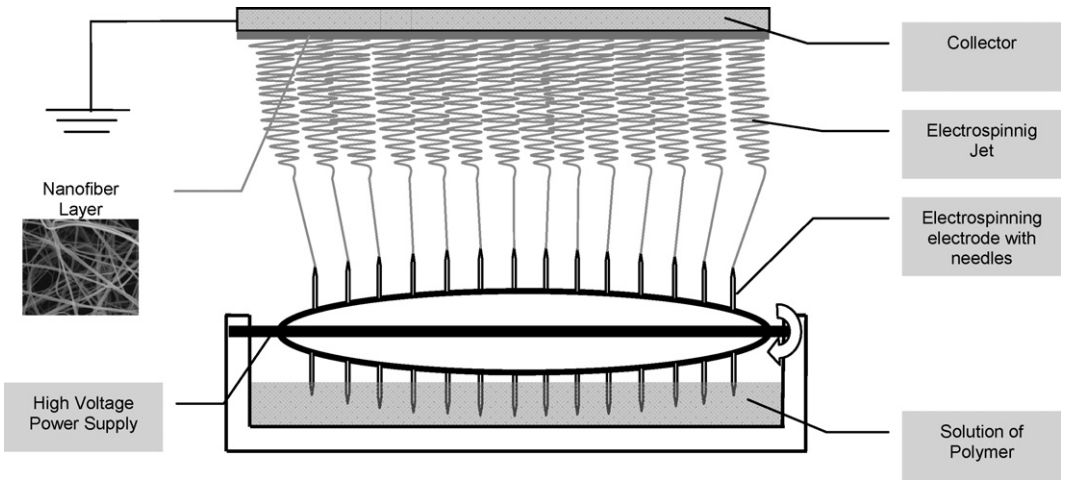

Fig. 1. Scheme of the electrospinning setup.

(Penta, min 99.0%) and dimethylformamide p.a. (Penta, min 99.5%) (volume ratio 3:1) and the weight concentration was adjusted to 15% (w/v). The prepared solution was stirred at 40 °C for 8 h and then it was cooled down to the ambient temperature. Electric conductivity was adjusted to 75 μS/cm (Gryf 156) by tetraethylamonium-bromide (Aldrich, p.a., it possesses relatively good solubility in dimethylformamide in comparison with others common salts).

Polyurethane solution was prepared by dissolving polyurethane granulate (Desmopan DP 2590A, Bayer Material Science) in mixed methylisobutylketone and dimethylformamide (volume ratio 1:3), the weight concentration was adjusted to 15.5% (w/v) and the electric conductivity to 150 μS/cm by tetraethylamonium-bromide. The solution was stirred at 50 °C for 12 h and cooled to the ambient temperature after complete dissolving.

Nanofibrous layers were prepared from fresh solutions by electrospinning. The used equipment (Elmarco) depicted in Fig. 1 involves the steel rotation spinning electrode with needles and the steel cylinder as the collecting electrode. The rotating spinning electrode is immersed to the solution of a polymer and the process of nanofiber formation starts with first drops on needles in the dead center of the rotation spinning electrode.

The electric voltage 75 kV (Matsusada DC power supply), temperature between 20 and 25 °C, relative humidity between 25 and 35% and the electrode spinning rate 8 min^{-1} were used for the electrospinning process.

The membrane was prepared by the hot-pressing method using 0.5 mm thick individual nanofibrous layers. The pressing power was 600 kN/m^2 and the temperature 80 °C. Final membrane density was ~120 g/m^3 for polystyrene (PS) and 420 g/m^3 for polyurethane (PU). In an initial series of samples the membrane was prepared by the hot-pressing method on the pad consisted of polypropylene and gelatine.

2.2. Characterization

Structural description of the produced materials was performed with scanning electron microscope TESCAN – Vega II LSH. The membranes were sputtered with Au/Pt in plasma (approximately 5 nm) and analyzed for their fiber diameter.

Textural properties of the membranes were evaluated by using standard textural methods based on high-pressure mercury porosimetry (AutoPore III, Micromeritics, USA), physical adsorption of nitrogen (ASAP 2050, Micromeritics, USA) at 77 K and helium pycnometry (AccuPyc 1330, Micromeritics, USA). To guarantee the precision of the obtained data purities of used nitrogen and helium (Technoplyn, Linde) were 99.9995%. Before analysis all samples were dried at 50 °C for 24 h in vacuum (0.1 Pa).

2.3. Binary counter-current isobaric gas diffusion measurements

The diffusion experiments were performed in a Graham's diffusion cell [24–27] (Fig. 2). The Graham's diffusion cell, based on the validity of the Graham's law [28], represents a modification version of the well-known Wicke-Kallenbach diffusion cell [29]. The diffusion cell depicted in Fig. 2 consists of two identical flow-through compartments separated by an impermeable disc with cylindrical holes. Volume of the each compartment was 150 cm^3. Tested membranes were forced into the impermeable disc by using a sealing O-ring. The absence of gaps between membranes and the O-ring as well as between the O-ring and the surface of the disc holes was verified by replacing the tested membranes with identically sized metallic pellets. Both sides of sample were flushed with a different gas stream with sufficiently high velocity to eliminate the influence of the external diffusion resistance. The optimum gas flow rate in both compartments, 150 cm^3/min, was optimized in a series of preliminary experiments. Lower flow rates resulted in changes of the measured diffusion flux densities while higher flow rates reveal no effect. All diffusion tests in the Graham's cell were performed under normal temperature and pressure.

Tested membrane sample of a circle shape (diameters equal to 5 mm) were prepared either from the polystyrene or polyurethane nonwoven mats, or their combinations, by using a die cutting tool. The sample test area clamped in the impermeable disc exposed a circular area of 0.196 cm^2 to the upper and lower gas streams. All counter-current gas diffusion measurements had to be performed very carefully owing to soft and easily deformable structure of membranes.

During the gas diffusion measurements gases flowed steadily through the upper and lower cell chambers until the steady state was established. Then the gas inlet and outlet in one of the cell chambers (typically the lower chamber) were closed and the net volumetric diffusion flux was determined by a digital bubble flowmeter (Optiflow HFM 570, Agilent Technologies, USA) connected to the bottom cell compartment (see Fig. 2). The heavier gas was always fed into the upper cell compartment. Three not adsorbing gases, nitrogen, helium and argon (99.99% purity, Messer Technogas) were used for the diffusion tests.

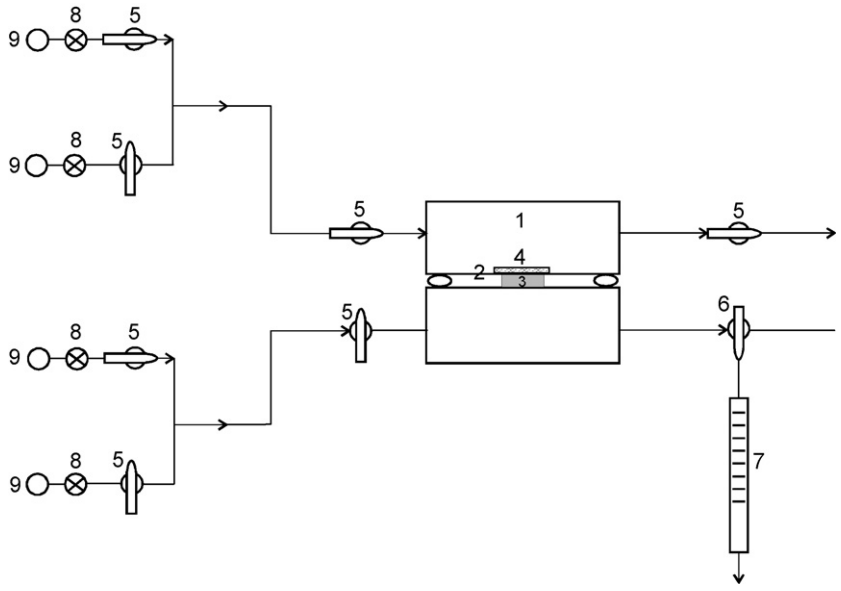

Fig. 2. Graham's diffusion cell set-up: (1)—diffusion cell, (2)—impermeable disc, (3)—tested membranes, (4)—sealing ring, (5)—valves, (6)—three-way valve, (7)—digital bubble flowmeter, (8)—mass flow controllers and (9)—pressure cylinders with gases.

3. Results and discussion

3.1. Characterization of membranes morphology

SEM images in Fig. 3 show typical morphologies of the prepared electrospun polystyrene (PS) and polyurethane (PU) membranes. It can be seen that the PU membrane comprises predominantly straight fibers in comparison with the PS membrane. In the latter case variously curved fibers can be easily detected. Fig. 4 indicates the distribution of electrospun fiber diameter. The statistical distribution of the diameter was calculated from 40 separate fibers. In both cases fibers with diameter between 50 and 450 nm were detected. Frequency distribution of the PS membrane is narrower with a maximum at 250 nm in comparison with frequency distribution of the PU membrane with a broad maximum between 250 and 350 nm and bigger portion of border diameters (50 and 450 nm).

Textural properties of the prepared PS and PU membranes are summarized in Table 1, where S_{BET} denotes the inner surface area determined from the classic BET isotherm, S_{meso} is the surface area of mesopores determined from the modified (three parametric) BET isotherm, V_{micro} is the micropore volume determined from the modified (three parametric) BET isotherm, V_{intr} states for the total intrusion volume from mercury porosimetry, ε denotes the porosity calculated from the apparent density, ρ_{Hg}, and the true density, ρ_{He}, according to $\varepsilon = 1 - \rho_{Hg}/\rho_{He}$.

It is known that the electrospun nanofiber membranes could be produced over a wide range of porosities [14], from nearly non-porous to highly porous structures. The samples presented here reveal the porosity of 71% (PU) and 89% (PS). For texture result evaluation the widely used high-pressure mercury porosimetry technique as same as the nitrogen adsorption method which are generally applicable and appropriate [15,30,31] not only for the pore-size distribution (PSD) determination in the solid-state polymeric materials were applied. From the obtained textural results it is clearly seen that the surface area of both membranes is rather low. In comparison with the PU membrane the PS one possesses a higher BET surface area together with higher volume of micropores. The pore-size distributions (PSDs) which were evaluated from the adsorption branches of nitrogen isotherms by the advanced Barret-Joyner-Halenda (BJH) method [32] are shown in Fig. 5a. The PSD curve for the PS membrane is located well above the curve for the PU

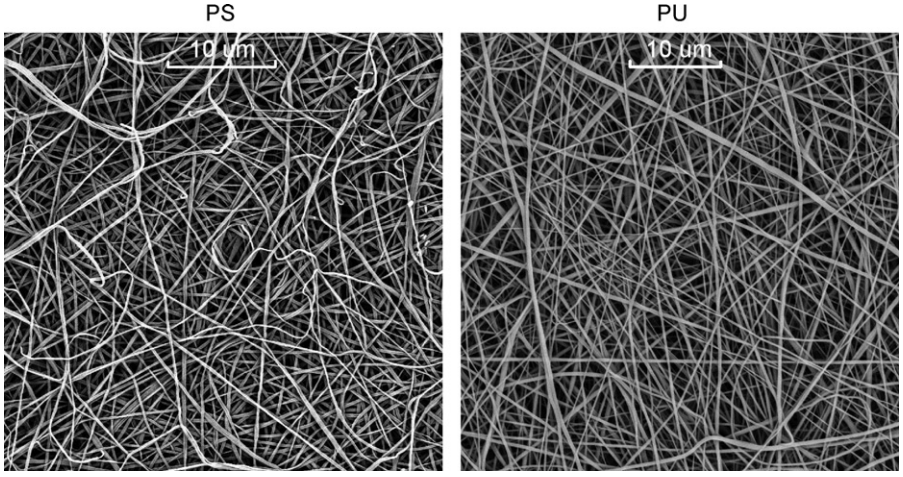

Fig. 3. SEM micrographs of prepared polystyrene (PS) and polyurethane (PU) membranes.

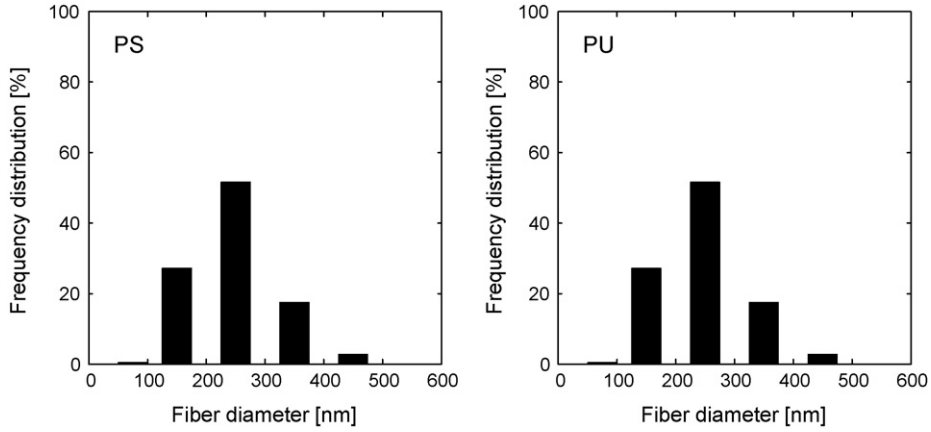

Fig. 4. Fiber diameter distributions of the prepared polystyrene (PS) and polyurethane (PU) membranes.

Table 1
Textural properties of prepared electrospun membranes.

Membrane	S_{BET} [m^2/g]	S_{meso} [m^2/g]	V_{micro} [mm^3/g]	V_{intr} [cm^3/g]	ρ_{He} [g/cm^3]	ρ_{Hg} [g/cm^3]	ε [–]
PS	9.2	7.9	0.8	5.83	1.05	0.11	0.89
PU	3.8	3.4	0.16	2.00	1.26	0.36	0.71

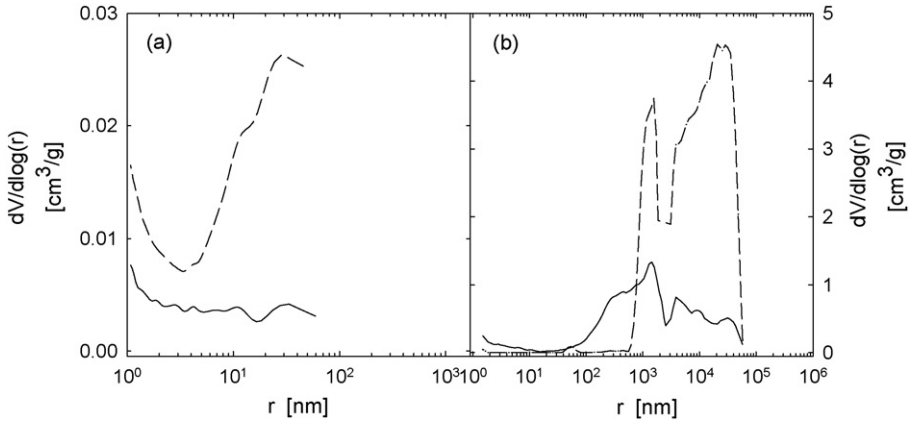

Fig. 5. (a) Pore-size distribution evaluated from the adsorption branch of nitrogen isotherm and (b) pore-size distribution evaluated from the high-pressure mercury porosimetry. PS membrane (– – –) and PU membrane (—).

membrane. It corresponds to the higher surface area and micropore volume. PS membranes reveal bidisperse pore-size distribution with maxima at 24 nm and below 2 nm. The PU membranes possess polydisperse pore-size distribution with unnoticeable maxima at 30, 10 and less than 2 nm.

Pore-size distribution curves obtained from the high-pressure mercury porosimetry are depicted for both membranes in Fig. 5b. Owing to the limitation when mercury is pressed into the very small pores, the minimum pore radius which can be measured by this method is approximately 3 nm. However, contrary to the nitrogen adsorption technique the mercury porosimetry enables a precise determination of larger pores in the range 10–100 μm (for more details of both techniques see [33]). It can be easily seen that pore-size distribution of PS membrane is shifted toward wider pores between 0.6 and 70 μm with r_{max} at 30 μm in comparison with PSD of the PU membrane between 70 nm and 70 μm with noticeable r_{max} at 2 μm. The pore-size distribution curve of the PS membrane is located above the PU curve, which corresponds to the higher total intrusion volume (5.8 cm^3/g) for the PS membrane and 2 cm^3/g for the PU membrane.

3.2. Gas diffusion transport

Optimization of the electrospinning process allowed preparation of self-supported membranes and a pad typical for such structures might has been finally avoided. Initially a series of samples on this standard support were also produced. For the membrane homogeneity characterization four identical samples from different sections of the raw polystyrene membrane sheet (10 cm × 10 cm) were taken. The net diffusion molar flux densities, N^d, summarized in Table 2 were measured for the two gas pairs N_2/He and Ar/He which differ in an agreement with the Graham's law $N_1^d/N_2^d = -\sqrt{M_2/M_1}$. The differences in the net diffusion molar

Table 2
Homogeneity of the prepared polystyrene membranes.

#	1	2	3	4	Mean	Standard deviation
$N^d_{N_2/He}$ [μmol/cm^2/s]	12.72	12.54	12.70	12.88	12.71	0.108
$N^d_{Ar/He}$ [μmol/cm^2/s]	16.40	16.08	16.42	16.27	16.29	0.121

Table 3
Net diffusion molar flux densities obtained from the Graham's diffusion cell.

	Polystyrene with pad	Polystyrene without pad	Polyurethane with pad	Polyurethane without pad
$N^d_{N_2/He}$ [μmol/cm²/s]	12.71	15.71	16.26	18.58
$N^d_{Ar/He}$ [μmol/cm²/s]	16.29	20.61	20.19	26.27

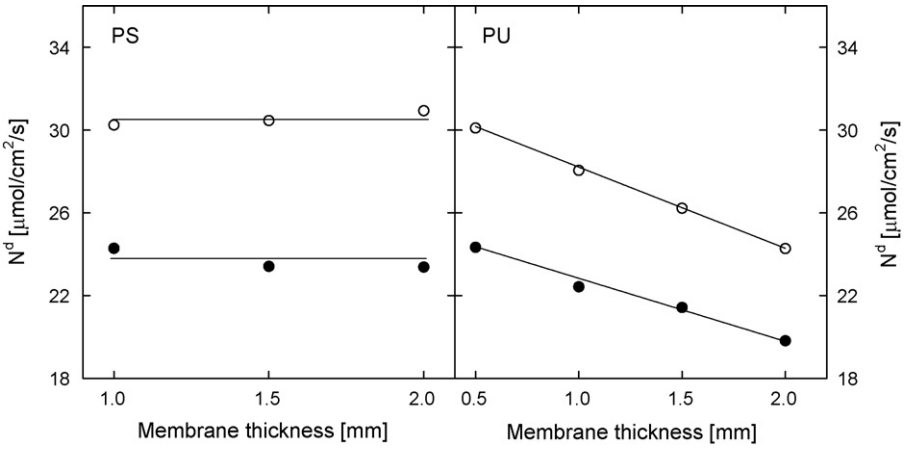

Fig. 6. Dependence of the net diffusion molar flux densities on membrane thickness for polystyrene (PS) and polyurethane (PU) membranes. (○)—argon/helium gas pair and (●)—nitrogen/helium gas pair.

flux densities of membranes do not exceed 3% and hence, their homogeneity can be assessed as very good.

The net diffusion molar flux densities were measured for polystyrene and polyurethane membranes prepared with and without the pad to evaluate the differences of diffusion properties. Obtained results are summarized in Table 3. It can be seen that the net diffusion molar flux densities for the pair N_2/He varied from 12.71 to 18.58 μmol/cm²/s and for pair Ar/He ranged from 16.29 to 26.27 μmol/cm²/s. Soukup et al. [26] found that for conventionally industrial catalysts the net diffusion molar flux densities exhibit about ten times lower magnitudes, which is quite essential for the catalytic reaction course and reaction rates. It is obvious that the membranes prepared on the pad reveal higher diffusion flux resistance (which is inversely proportional to the diffusion flux density) in comparison with those prepared without the pad. The diffusion resistance data of polystyrene and polyurethane membranes were assessed by using the inert gas binaries nitrogen/helium and argon/helium. Thus, the unwanted adsorption and so far the insufficiently mathematically described surface diffusion transport were eliminated.

Fig. 6 shows dependence of the net diffusion molar flux densities on the membrane thickness. It appears that the diffusion resistance of the polyurethane membrane was much higher than that of the polystyrene membranes of the same thickness. The diffusion flow resistance increased with the membrane thickness in the whole range of areal weights for the polyurethane membranes. On the other hand, it remained nearly unchanged for the polystyrene membranes. It can be explained by the lower area weight of the PS membranes which, as seen in Table 4, was approximately three times lower than for the polyurethane membranes.

Table 4
Areal weights of the tested membranes.

Thickness [mm]	Polyurethane membranes Areal weight [g/m²]	Polystyrene membranes Areal weight [g/m²]
0.5	100.33	34.22
1.0	216.00	70.89
1.5	342.56	98.22
2.0	431.33	135.56

Table 5
Net diffusion molar flux densities for polyurethane and polystyrene membranes prepared by the different techniques.

	PU1	PU2	PU3	PS1	PS2	PS3
$N^d_{N_2/He}$ [μmol/cm²/s]	19.83	19.97	20.18	24.10	24.58	24.38
$N^d_{Ar/He}$ [μmol/cm²/s]	24.25	24.56	23.29	29.94	30.04	30.71

Net diffusion molar flux densities for polyurethane and polystyrene membranes prepared under different process conditions are given in Table 5. Thicknesses of all tested membranes were identical (2 mm). PU1 and PS1 denote for polyurethane and polystyrene membranes with thicknesses of 2 mm; PU2 and PS2 are membranes prepared by pressing (600 kN/m², 80 °C) four PU and PS sheets with 0.5 thickness each; PU3 and PS3 are membranes prepared by pressing (600 kN/m², 80 °C) two PU and PS sheets with 1 mm thickness. It clearly appears from Table 5 that the diffusion transport properties of the membranes are completely independent on the post-electrospinning membrane preparation technique. Thus, the pore structure is not significantly affected by the post-electrospinning manufacturing. This result is important for other technology.

3.3. Sandwich membrane structure

The sandwich membrane prepared from the three individual membrane layers (each with thickness of 2 mm) arranged in order of PS–PU–PS was also tested. Table 6 exhibits the net diffusion molar flux densities for PS–PU–PS sandwich in comparison with pure PS and PU membranes of the same thicknesses. The diffusion

Table 6
Comparison of the net diffusion molar flux densities for individual PS and PU membranes with PS–PU–PS sandwich membrane.

	Polystyrene membrane	Polyurethane membrane	Sandwich membrane PS–PU–PS
$N^d_{N_2/He}$ [μmol/cm²/s]	24.10	19.83	18.51
$N^d_{Ar/He}$ [μmol/cm²/s]	29.94	24.25	23.26

resistance of the sandwich membrane correlates well with the diffusion resistance of the pure PU membrane. It is obvious that the PU membrane with the higher areal weight (as well as the higher diffusion flux resistance) controlled the total diffusion flux resistance of the PS–PU–PS sandwich membrane and that the diffusion transport through the PU membrane is the rate determining step.

4. Conclusion

Electrospun nanofibrous layers finalized and used as membranes have been discussed in light of their gas transport characteristics. It was found that the diffusion resistance of the PU membranes was much higher than that of the PS membranes of the same thicknesses and for PU membranes the diffusion flow resistance increased with the membrane thickness contrary to PS membranes. Therefore, the diffusion resistance of the pure PU membrane controlled the total diffusion flux resistance of the PS–PU–PS sandwich membrane and that the diffusion transport through the PU membrane is the rate determining step. These properties were related with their structural and morphological features. It is believed that this knowledge might be of great importance due to enormous application potential of such unique materials. The major fields are catalysis, filtration, protective masks, tissue engineering, wound care, and drug delivery.

Acknowledgements

The financial support of Grant Agency of the Czech Republic (GA104/09/0694) and the Academy of Sciences of the Czech Republic, project No. KAN400720701 is gratefully acknowledged.

References

[1] M. Stasiak, C. Röben, N. Rosenberger, F. Schleth, A. Studer, A. Greiner, J.H. Wendorff, Polymer 48 (2007) 5208.
[2] X.J. Huang, D. Ge, Z.K. Xu, Eur. Polym. J. 43 (2007) 3710.
[3] L.S. Wan, B.B. Ke, Z.K. Xu, Enzyme Microb. Technol. 42 (2008) 332.
[4] K. Ebert, G. Bengtson, R. Just, M. Oehring, D. Fritsch, Appl. Catal. A: Gen. 346 (2008) 72.
[5] M.M. Demir, M.A. Gulgun, Y.Z. Menceloglu, B. Erman, S.S. Abramchuk, E.E. Makhaeva, A.R. Khokhlov, V.G. Matveeva, M.G. Sulman, Macromolecules 37 (2004) 1787.
[6] P.N. Shah, R.L. Manthe, S.T. Lopina, Y.H. Yun, Polymer 50 (2009) 2281.
[7] S.F. Li, W.T. Wu, Biochem. Eng. J. 45 (2009) 48.
[8] K.T. Shalumon, N.S. Binulal, N. Selvamurugan, S.V. Nair, D. Menon, T. Furuike, H. Tamura, R. Jaykumar, Carbohyd. Polym. 77 (2009) 863.
[9] K. Yoon, B.S. Hsiao, B. Chu, J. Membr. Sci. 338 (2009) 145.
[10] P. Rujitanaroj, N. Pimpha, P. Pubaphol, Polymer 49 (2008) 4723.
[11] S.F. Li, J.P. Chen, W.T. Wu, J. Mol. Catal. B: Enzym. 47 (2007) 117.
[12] G. Ren, X. Xu, Q. Liu, J. Cheng, X. Yuan, L. Wu, Y. Wan, React. Func. Polym. 66 (2006) 1559.
[13] G.C. Burger, B.S. Hsiao, B. Chu, Annu. Rev. Mater. Res. 23 (2006) 333.
[14] P. Gibson, H. Schreuder-Gibson, D. Rivin, Colloid Surf. A 187–188 (2001) 469.
[15] Y.J. Ryu, H.Y. Kim, K.H. Lee, H.C. Park, D.R. Lee, Eur. Polym. J. 39 (2003) 1883.
[16] R.S. Barhate, C.K. Loong, S. Ramakrishna, J. Membr. Sci. 283 (2006) 209.
[17] S. Lee, S.K. Obendorf, Fibers Polym. 8 (2007) 501.
[18] D.R. Nisbet, A.E. Rodda, D.I. Finkelstein, M.K. Horne, Colloid Surf. B: Biol. 71 (2009) 1.
[19] S. Ramakrishna, K. Fujihara, An Introduction to Electrospinning and Nanofibers, World Scientific Publishing Ltd, Singapore, 2005.
[20] A. Greiner, J.H. Wendorff, Chem. Int. Ed. 46 (2007) 5670.
[21] T. Subbiah, G.S. Bhat, R.W. Tock, S. Parameswaran, S.S. Ramkumar, J. Appl. Polym. Sci. 96 (2005) 557.
[22] S. Park, K. Park, H. Yoon, J. Son, T. Min, G. Kim, Polym. Int. 56 (2007) 1361.
[23] T. Han, D.H. Reneker, A.L. Yarin, Polymer 48 (2007) 6064.
[24] J. Valuš, P. Schneider, Appl. Catal. 1 (1981) 355.
[25] O. Šolcová, H. Šnajdaufová, P. Schneider, Chem. Eng. Sci. 56 (2001) 5231.
[26] K. Soukup, P. Schneider, O. Šolcová, Chem. Eng. Sci. 63 (2008) 1003.
[27] K. Soukup, P. Schneider, O. Šolcová, Chem. Eng. Sci. 63 (2008) 4490.
[28] T. Graham, London-Edinburgh Philos. Mag. J. Sci. 2 (1833) 269.
[29] E. Wicke, R. Kallenbach, Kolloid Zeitschrift 97 (1941) 135.
[30] R. Zaleski, V. Stefaniak, M. Maciejewska, J. Goworek, J. Porous Mater. 16 (2009) 691.
[31] K. Soukupova, A. Sassi, K. Jerabek, React. Funct. Polym. 69 (2009) 353.
[32] E.P. Barrett, L.G. Joyner, P.H. Halenda, J. Am. Chem. Soc. 73 (1951) 373.
[33] D.M. Rutheven, Principles of Adsorption and Adsorption Processes, A Wiley—Interscience Publication, New York, 1984.